Emission cross sections of excited fragments produced by electron impact on BCl_3

Ikuo Tokue, Mikiko Kudo, Masanobu Kusakabe, Tomohisa Honda, and Yoshio Ito
Department of Chemistry, Faculty of Science, Niigata University, Ikarashi, Niigata 950-21, Japan

(Received 29 January 1992; accepted 10 March 1992)

Emission spectra in the 190–600 nm region produced by electron impact on BCl_3 have been studied up to 110 eV. Emission cross sections of the $B(2s2p^2\ ^2D–2p\ ^2P^0)$ and $B(3s\ ^2S–2p\ ^2P^0)$ lines and the $BCl(A\ ^1\Pi–X\ ^1\Sigma^+)$ band are evaluated to be 4.9 ± 1.0, 4.5 ± 0.7, and $(1.9 \pm 0.3) \times 10^{-18}$ cm^2, respectively, at 100 eV. Formation cross sections of these species have been determined from the analysis of their fluorescence decaying curves. Two continuous emissions observed in the 230–380 and 400–580 nm regions are attributed to the BCl_2^* band. The fluorescence lifetime of BCl_2^* in the 300–342 nm region is obtained to be 1.65 ± 0.2 μs, which is nearly independent of the wavelength.

I. INTRODUCTION

Boron trichloride (BCl_3) is commonly used for the deposition of boron atom and for the plasma etching of aluminum and aluminum oxide in microelectronics fabrication. Dissociation processes of BCl_3 are of interest for diagnostics of reactive plasma systems including this molecule. The $BCl(A\ ^1\Pi–X\ ^1\Sigma^+)$ emission produced from BCl_3 has been relatively well studied,[1–3] thus spectroscopic information of BCl detected by laser-induced fluorescence[4,5] (LIF) has been used to probe the characteristics of BCl_3 radio-frequency discharges.[6,7]

Dessaux, Goudmand, and Pannetier[8] observed ultraviolet chemiluminescences from the chemical reaction of $H + BCl_3$ and assigned two BCl_2^* emissions. Later, Suto *et al.*[9] measured the absorption and fluorescence cross sections of BCl_3 in the vacuum ultraviolet and determined the fluorescence lifetime in the 460–660 nm region and the quenching rate constant of BCl_2^*.

In the electron impact of BCl_3, Hesser[10] observed the intense $BCl(A–X)$ emission near 272 nm, as well as a weak emission extending from 190 to 320 nm, and determined the fluorescence lifetime of the $BCl(A)$ state. In order to investigate primary processes in BCl_3 discharges, it is necessary to measure the emission cross section (ECS) of fragments produced by electron impact. The ECS of the $BCl(A–X)$ transition produced by electron impact on BCl_3 was measured up to 50 eV.[11] However, there has been only little information about the formation cross section (FCS) of fragments produced by electron impact on BCl_3; the FCS means the cross section for direct formation of the product state. The optical emission from a fragment is generally induced not only by direct excitation to the emitting state but also by cascading from higher excited states. In this circumstance, the ECS is not necessarily always equal to the FCS of the upper state for the corresponding emission.

This paper describes the measurement of ECSs and fluorescence lifetimes of the $B(2s2p^2\ ^2D–2p\ ^2P^0)$ and $B(3s\ ^2S–2p\ ^2P^0)$ lines and the $BCl(A\ ^1\Pi–X\ ^1\Sigma^+)$ band produced by electron impact on BCl_3 under the single-collision condition. Furthermore, the FCSs of radiative states concerning these emissions have been evaluated with the aid of the results in fluorescence decaying curves and fluorescence onsets. Broad emissions have also been observed in the 230–380 and 400–580 nm regions. Although very little is known about the spectroscopic data, the emitters for these bands have been attributed to BCl_2^*. The potential energies for these emitting states of BCl_2 are estimated from their fluorescence onsets.

II. EXPERIMENT

A. Apparatus

Emission cross sections (ECSs) have been measured by a combination of an effusive molecular beam and an electron beam in conjunction with a monochromator–photomultiplier detection system. Figure 1 shows a block diagram of the apparatus, which consists of a collision chamber and an electron-beam source. Two chambers were evacuated differentially by each oil diffusion pump of 500 l/s with a water baffle and a liquid-nitrogen trap. Target gases flowed out vertically to the collision chamber forming the effusive molecular beam through a multicapillary array (MCA) of 5 mm diam; the internal diameter and length of a capillary were 0.13 and 5 mm, respectively. The gas pressure at the upper stream of the MCA, where the flow is sufficiently viscous, was measured with an MKS Baratron (model 270C). When nitrogen gas was introduced into the collision chamber, the ambient pressure of the chamber measured by an ionization vacuum gauge was kept under 1.2 mPa and the electron-beam source was evacuated to 0.55 mPa. The molecular beam crossed the electron beam perpendicularly about 7 mm downstream from the MCA. The samples of BCl_3 (99.9999%) and N_2 (99.9995%) obtained from Nippon Sanso were used without further purification.

The electron beam was produced by a gun equipped with a thoria-coated tungsten filament. The negative potential from 0 to 110 eV was applied to the filament. The accelerated electrons were focused by an einzel lens onto the molecular beam and a coaxial magnetic field of about 50 G was used for additional collimation. The energy spread of the electron beam was estimated to be 1 eV [full width at half maximum (FWHM)] and the electron-beam current measured by a deep Faraday cup varied from 10 to 70 μA. The

 0021-9606/92/128889-08$06.00

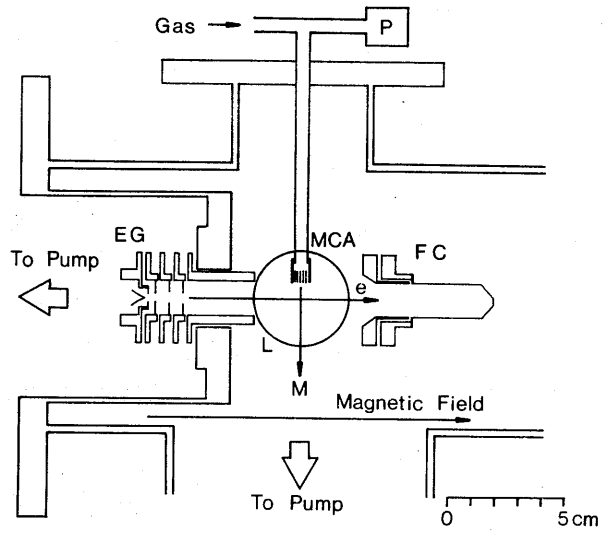

FIG. 1. A schematic diagram of the apparatus: electron gun (EG), Faraday cup (FC), multicapillary array (MCA), quartz lens (L), and MKS Baratron (P).

emitted photons were observed in a direction perpendicular to both the electron beam and the molecular beam.

Experimental procedures for the lifetime and ECS measurements will be discussed in the following sections.

B. Lifetime measurements

When target molecules are excited by collisions with pulsed electrons, they can cause several decay processes, some of which lead to dissociation to radiative fragments. The experimental setup for measurements of the fluorescence lifetime has been described elsewhere.[12] In brief, the electron beam was chopped with a repetition frequency of 125 or 250 kHz (a pulse width of 100 ns) and the decay curve was obtained by a delayed coincidence method with a combination of a time-to-amplitude converter and a multichannel analyzer. The cutoff of the electron beam was tested by measuring the lifetime of 1.72 ns for the $3p(^1P_0)$ state of helium.[13] The time profile of the He($3p\ ^1P_0$–$2s\ ^1S$) line was nearly exponential and the cutoff time was estimated to be less than 13 ns.

In general, the measurement of the fragments with long lifetimes ($\geqslant 1\ \mu s$) by using a monochromator is difficult since the emitters can escape from the viewing region in the collision chamber before fluorescence decay. In the present experiment, the entrance slit of the monochromator was arranged perpendicular to the electron beam. In this case the radiative fragments flying parallel to the slit height are most serious on the assumption that the fragments are distributed cylindrically with respect to the electron beam. In order to estimate this escaping effect, the decay curves were measured with a slit height of 5–10 mm. The obtained lifetimes did not depend on the slit height. Therefore, the escaping effect of the fragments from the viewing region is negligible.

Time-dependent profiles of the delayed coincidence curve for fragments from BCl_3 were apparently nonexponential. Therefore, the decay curves were analyzed by a nonlinear least-square-fitting procedure as a superposition of three decaying components. After the cutoff of excitation ($t > 0$), the dependence of the photon count rate $R(\lambda,t)$ at the wavelength λ is assumed to be represented by the following fitting function:

$$R(\lambda,t) = C_0(\lambda) + \sum_{k=1}^{3} C_k(\lambda)\exp[-t/\tau_k(\lambda)]. \qquad (1)$$

Here, $C_0(\lambda)$ is a background constant, and $C_k(\lambda)$ and $\tau(\lambda)$ are the amplitude at $t = 0$ and the fluorescence lifetime, respectively, for the k component. The fitting function was convoluted with the time profile of the detection system, which was estimated by measuring the decay curve for the He($3p\ ^1P_0$–$2s\ ^1S$) line at 501.6 nm.[13] After subtraction of the background constant, the observed decay curves from fragments were fitted by using six parameters for amplitude and lifetime. Twice the standard deviations of the fitting parameters given by the fitting routine were adopted as the errors of the parameters.

C. Measurements of emission cross sections

When the fragments produced by the electrons of the energy E emit the photons of the wavelength λ, the photon count rate $R(\lambda,E)$ is given by[14]

$$R(\lambda,E) = n_T \cdot I(E)/e \cdot \sigma(\lambda,E) \cdot \epsilon(\lambda) \cdot f(\lambda,E), \qquad (2)$$

where n_T is the density of the target molecules, $I(E)$ is the electron-beam current, and $\sigma(\lambda,E)$ and $\epsilon(\lambda)$ designate the ECS and the quantum efficiency of the photon-detection system, respectively, at the wavelength λ. The geometrical factor $f(\lambda,E)$ is defined as the ratio of the photon flux introduced to the entrance slit of monochromator to the total photon flux produced by the electron–molecule collision. This factor includes effects due to the anisotropy of fluorescence.

In the ECS measurement, a determination of the absolute values may include several sources of uncertainty; the major origins reported in the literature[15] are a determination of the target gas density n_T and the absolute sensitivity of the photon-detection system $\epsilon(\lambda) \cdot f(\lambda,E)$. Nevertheless, for conventional measurements, it is possible to avoid determinations of these absolute values if there is an appropriate standard of which ECS is known with sufficient accuracy. The systematic uncertainties that may be included in each absolute value are canceled by applying the conventional measurements to both the target and the standard. Thus, ECSs of the target molecule are obtained accurately.

Helium or N_2 is very suitable for the standard gas of this kind of experiment. Although the uncertainty of the ECS values of He neutral lines has reached about 5% in the carefully organized experiment,[15] these He lines are relatively weak. In the present study, ECSs of the radiative fragments from BCl_3 have been evaluated on the basis of the ECS value of the 0–0 band of the N_2^+ ($B\ ^2\Sigma^+$–$X\ ^2\Sigma^+$) transition at 100 eV, $(1.74 \pm 0.17) \times 10^{-17}$ cm^2.[16] The ECS of the N_2^+ (B–X) band from N_2 gas was measured separately before and after the measurements for the fragments from BCl_3 gas. Thus, Eq. (2) is applied to both the N_2^+ (B–X) band and a fragment emission. When each ECS is integrated

over λ, the ECS of the fragment emission $\sigma(E) = \int \sigma(\lambda,E)d\lambda$ is given by the following ratio:

$$\sigma_B(E) = \sigma_N(E) \cdot \frac{n_N}{n_B} \cdot \frac{I_N(E)}{I_B(E)} \cdot \frac{\int R(\lambda_B,E)/[\epsilon(\lambda_B)\cdot f(\lambda_B,E)]d\lambda_B}{\int R(\lambda_N,E)/[\epsilon(\lambda_N)\cdot f(\lambda_N,E)]d\lambda_N}, \quad (3)$$

where the subscripts B and N denote BCl_3 and N_2, respectively, and σ_N means the ECS of the 0–0 band of the N_2^+ (B–X) transition.

(*i*) *The geometrical factor* $f(\lambda,E)$. Although the form of the light-emitting volume almost coincides with the form of the electron beam, the light-emitting volume expands slightly because of the translational motion of the fragments with finite lifetimes of the radiative states. The viewing angle of the monochromator was sufficiently large to capture the whole collision volume, and then the escape of N_2 and the fragments from the viewing region is negligible as discussed in Sec. II B.

The polarization of the N_2^+ ($B\,^2\Sigma^+$–$X\,^2\Sigma^+$) band has been found to be less than 5% up to 3 keV.[16] No polarization of the BCl($A\,^1\Pi$–$X\,^1\Sigma^+$) band has been confirmed by laser-induced fluorescence.[5] The polarization of the B($3s\,^2S$–$^2P^0$) line is theoretically zero, whereas the polarization of the B($2s2p^2\,^2D$–$^2P^0$) line is not known. Nevertheless, polarization effects for emissions from fragments of polyatomic molecules are known to be negligibly small. Thus, any effects due to the anisotropy of fluorescence are neglected.

Consequently, the ratio of the geometrical factor f_B/f_N is assumed to be unity for all the emissions. The uncertainty for this assumption is estimated to be 0%–5%.

(*ii*) *The relative quantum efficiency* $\epsilon(\lambda)$. In the ECS measurement, the photon-detection system consists of two quartz lenses, a monochromator (Ritsu CT-30N), a photomultiplier (Hamamatsu R585), and photon counting electronics (Hamamatsu C1230).

The relative sensitivity of the total photon-detection system was calibrated with a deuterium lamp in the 190–350 nm region and with a halogen lamp in the 250–600 nm region; the two curves for calibration are connected at 300 nm. The uncertainty of the relative sensitivity is estimated to be about 5% for 205–240 nm, 4% for 240–323 nm, and 3% for 323–600 nm. The estimations of these uncertainties are based on the reproducibility through repeated measurements.

(*iii*) *The ratio of the target gas density*. The target gas was introduced into the collision chamber via the MCA. Under conditions of molecular flow in the capillary, the pressure in the gas reservoir is directly related to the flow rate.[17] At these low pressures, data aquisition, however, will be significantly affected by low counting rates and long accumulation times. In the present experiment, the ECSs were measured at higher pressures, where collisions affect the spatial distribution of target flow. Moreover, under these conditions, the relative target density at the collision region cannot be expressed by a simple relation of the pressure at gas reservoir.

The change in the spatial distribution of the target beam at the collision region may cause a serious error. Thus, the

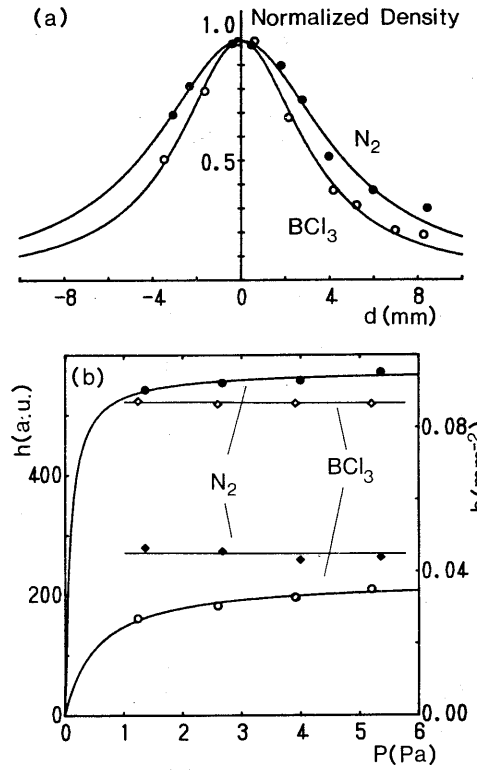

FIG. 2. (a) Density profiles of N_2 (●) and BCl_3 (○) along the line perpendicular to the electron-beam axis and 7 mm downstream from the MCA tip measured at $P = 2.6$ Pa: the curves represent the best-fitted functions of a Lorentz type. (b) Pressure dependence of the parameters h for N_2 (●) and BCl_3 (○) and b for N_2 (◆) and BCl_3 (◇): the fitting function for h is $h_\infty P/(A+P)$, where h_∞ means the h value at $P = \infty$.

spatial density distribution of the gas beam was measured in order to confirm that the region of uniform density was much larger than the geometrical cross section of the electron beam ($\approx$3 mm diameter). The density profiles of the N_2 and BCl_3 beams were monitored by observing the emission intensities of the N_2^+ (B–X) band and the B(^2D–$^2P^0$) line, respectively. The position of the MCA was varied for both sides with respect to the center of the electron beam. Figure 2(a) shows typical profiles of N_2 and BCl_3 beams at a gas pressure (P) of 2.6 Pa measured by MKS Baratron: the photon counting rate normalized at the peak vs the distance (d) from the electron-beam center. It can be found that the density of the molecular beam is nearly uniform at the collision region, $|d| \leqslant 1.5$ mm in Fig. 2(a), and that the profile of the lighter molecule is broader. These profiles, which should be represented by a convolution of the molecular-beam distribution with that of the electron beam, were fitted with a Lorentz-type function $h/(1 + b\cdot d^2)$, where h and b are adjustable parameters. Applying the Lorentz function to the beam profiles, the ratio of the particle density at the collision region (peak) relative to the total flow is represented by $\sqrt{b}/\pi$. The pressure dependences of the parameters h and b are also displayed in Fig. 2(b).

The width parameters b for both N_2 and BCl_3 were nearly independent of the pressure. Figure 2(b) shows that the parameter h, which should be related to the photon

counting rate normalized by the target density R/n, depends on the pressure P. This dependence leads to the result that the target density at the collision region cannot be expressed by a simple relation of the pressure P measured by the MKS Baratron. On the assumption that the condition of the molecular flow is realized at the top of the MCA, the rate equations for the gas flow result in the following relation between the target density and the pressure P:

$$n \propto P^2/(A+P), \quad A=\frac{\pi r^4}{8lS\eta}\left(\frac{2\pi M}{RT}\right)^{1/2}, \tag{4}$$

where r and l represent the radius and length, respectively, of the gas introducing line; S means the effective cross section of the MCA; and η and M are the viscosity and molecular weight, respectively, of the target gas.

In the present measurement, the parameter A was determined by the pressure dependence of the h parameter, which is shown in Fig. 2(b). Thus, the ratio of n_B/n_N is represented by

$$\frac{n_N}{n_B}=\frac{\sqrt{b_N}}{\sqrt{b_B}}\cdot\frac{(A_B+P_B)}{P_B^2}\cdot\frac{P_N^2}{(A_N+P_N)}. \tag{5}$$

The uncertainty of the relative gas density thus evaluated is estimated to be 10%.

For the measurement of the emission thresholds for the radiative fragments from BCl_3, the energy scale of the incident electrons was calibrated against the onset (11.03 eV) of the N_2 ($C\,^3\Pi$–$B\,^3\Pi$) band and the onset (18.75 eV) of the N_2 ($B\,^2\Sigma^+$–$X\,^2\Sigma^+$) band which were produced from N_2 mixed in BCl_3 gas.[18] We found that the exposure of the electron gun and the Faraday cup to the corrosive BCl_3, even at low pressures in the mPa range, causes rapid drifts in the contact potential. Thus, the onsets of the N_2 and N_2^+ bands were checked frequently during the measurement.

III. RESULTS AND DISCUSSION

A. Emission spectra from fragments

Figure 3 shows the emission spectra resulting from dissociative excitation of BCl_3. Atomic lines (B, B^+, Cl, Cl^+), the BCl($A\,^1\Pi$–$^1\Sigma^+$) band, and continuous bands were observed. The tables of Zaidel, Prokof'ev, and Raiskii[19] have been used for the assignment of the various atomic lines. The peaks at 209 and 250 nm are assigned to the B($2s2p^2\,^2D$–$2p\,^2P^0$) and B($3s\,^2S$–$2p\,^2P^0$) lines, respectively.[11] The band at 272 nm is the well-known BCl($A\,^1\Pi$–$^1\Sigma^+$) system.[1-3]

The spectrum observed at the impact energy of 17 eV shows clearly continuous emissions in the 230–380 nm region with a maximum at 305 nm and in the 400–580 nm region with a maximum at 500 nm, which are very similar to the C and A bands, respectively, observed by Suto *et al.*[9] Moreover, a broad band at 350 nm is distinct from the continuous emission. This is confirmed by the dependence of their profiles on the impact energy. The 350 nm band seems to be the same as the B band observed by Suto *et al.*[9] Hence, we designate the three bands as the A, B, and C bands in accordance with them. The A band has been assigned as the BCl_2^* emission. Dessaux, Goudmand, and Pannetier[8] have

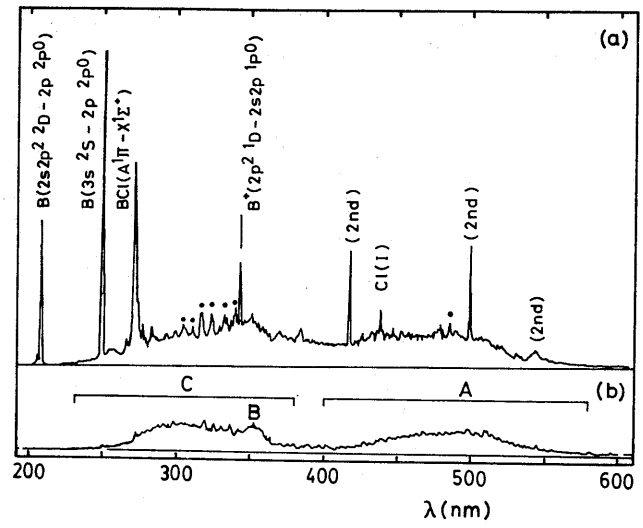

FIG. 3. Emission spectra of BCl_3 measured at electron energies of (a) 70 and (b) 17 eV with the 1.2 nm FWHM resolution with gas pressure of 20 Pa and beam current of 60 μA; the peaks indicated by the solid circles represent the emission from the impurity HCl. The variation of the optical sensitivity with the wavelength is not corrected.

observed the chemiluminescence spectrum from the reaction of H + BCl_3, which is assigned as two BCl_2^* emissions. On the basis of the spectral similarity between the B and C bands and the chemiluminescence specta, the B and C bands have been also assigned as the BCl_2^* transitions. The C band seems to be different from the emission in the 190–320 nm region observed by the electron impact of BCl_3.[10] The assignments for the A and C bands have been confirmed by the measurement of their emission thresholds, which will be described in Sec. III B. Vibrational structures of the B and C bands were assigned tentatively,[8] whereas no information on their electronic states have been reported yet.

The emission intensities of the B(^2D–$^2P^0$) and B(^2S–$^2P^0$) lines, the BCl(A–X) band, and BCl_2^* emissions at 330 and 468 nm were found to increase linearly with both the gas pressure in the 1.0–6.6 Pa range and the electron-beam current in the 1–70 μA range. This indicates that the excited states of B, BCl, and BCl_2 are produced via single collisions of parent molecules with electrons.

In Fig. 3, the line emission at 486 nm indicated by the solid circle is most likely the hydrogen Balmer-β line due to the impurity HCl, which could be produced by the reaction of BCl_3 with water adsorped on the wall of the gas handling system. Moreover, the peaks in the 300–340 nm region indicated by solid circles are assigned to the HCl^+ ($A\,^2\Sigma^+$–$X\,^2\Pi$) band.[20] The amount of HCl impurity was estimated to be less than 5% by comparing the emission intensity of the 486 nm peak with the ECS of the hydrogen Balmer-β line from HCl.[21]

B. Emission cross sections of fragments

Table I lists the ECSs of the B(^2D–$^2P^0$) line at 209 nm, the B(^2S–$^2P^0$) line at 250 nm, and the BCl(A–X) band at 272 nm obtained at an incident electron energy of 100 eV. The ECS of the BCl(A–X) band represents the integrated

TABLE I. Emission cross sections (σ) of fragments produced from BCl_3 at 100 eV.

Transition	λ[a] (nm)	σ (10^{-18} cm^2)
$B(2s2p^2\ ^2D\text{–}2p\ ^2P^0)$	208.9	4.9 ± 1.0
$B(3s\ ^2S\text{–}2p\ ^2P^0)$	249.7	4.5 ± 0.7
$BCl(A\ ^1\Pi\text{–}X\ ^1\Sigma^+)$[b]	271.5	1.9 ± 0.3

[a] The spectral band pass is 1.2 nm FWHM.
[b] Spectroscopically unresolved 0–0, 1–1 and 2–2 bands.

vibrational bands of the $\Delta v = 0$ sequence. Figure 4 plots the ECSs of the $B(^2D\text{–}^2P)$ and $B(^2S\text{–}^2P)$ lines and the $BCl(A\text{–}X)$ band against the incident electron energy. The ECSs of boron lines show very similar features: a first maximum around 27 eV, the second rise near 34 eV to reach an overall broad maximum around 80 eV. The maximum ECSs of the $B(^2D\text{–}^2P)$ and $B(^2S\text{–}^2P)$ lines are 5.0 ± 1.0 and $(4.7 \pm 0.7) \times 10^{-18}$ cm^2, respectively. The ECS of the $BCl(A\text{–}X)$ band rises to a first maximum around 23 eV and then rises again near 27 eV to reach its overall maximum around 41 eV. The maximum ECS at 41 eV is $(2.6 \pm 0.4) \times 10^{-18}$ cm^2, which is slightly larger than the value of $(2.3 \pm 0.4) \times 10^{-18}$ cm^2 measured by Jabbour, Mortus, and Becker.[11] No attempt was made to measure the absolute ECSs of the BCl_2^* emissions because of their broad features and overlapping with a number of atomic lines.

Excitation spectra of the radiative fragments near their thresholds were measured at 208.9, 249.6, 271.5, 318–333, and 467.4 nm with the 1.2 nm FWHM resolution. Figure 5 shows the excitation spectra near the onsets measured at 209, 250, 272, and 330 nm; the observed onset is indicated by a vertical line.

Table II lists the dissociation processes leading to formation of $B(2s2p^2\ ^2D)$, $B(3s\ ^2S)$, $B(3p\ ^2P^0)$, $BCl(A\ ^1\Pi)$, and BCl_2^* near their thresholds. The observed onsets are compared with the thresholds calculated by using the enthalpies of formation for the parent and related fragments[22,23] and the electronic energies of the excited states.[13,18] No electronic state has been assigned yet for BCl_2. Hence, the photon energies at the center of the BCl_2^* emissions were used for the excitation energies of the emitting states.

The onsets measured at 208.9 nm from $B(2s2p^2\ ^2D)$ are evaluated to be 17.7 ± 0.2 and 20.2 ± 0.5 eV. These values are in good agreement with the calculated thresholds for reactions (3) and (4), respectively, forming $B(^2D)$. On the other hand, the onsets for the $B(3s\ ^2S)$ state obtained at 249.6 nm are 17.7 ± 0.4 and 19.7 ± 0.3 eV, which are considerably higher than the calculated thresholds for reactions (1) and (2), respectively. Nevertheless, the observed onsets agree well with the thresholds calculated for reactions (5) and (6), respectively, forming $B(3p\ ^2P^0)$. This indicates that the $B(3s\ ^2S)$ state is produced via cascading of the $B(3p\ ^2P^0 \rightarrow 3s\ ^2S)$ transition. This conclusion is consistent with the result obtained from the fluorescence decaying curve of the $B(3s\ ^2S\text{–}2p\ ^2P)$ line, which will be discussed in Sec. III C. The third onset around 33 eV observed from both boron lines is probably attributed to the reactions

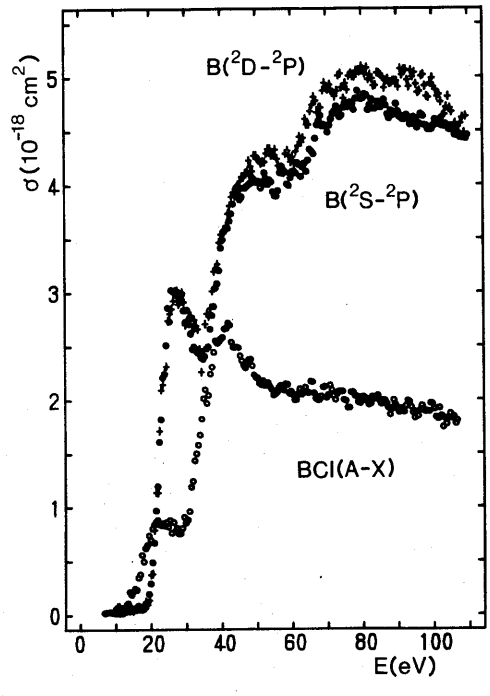

FIG. 4. The ECSs of the $B(^2D\text{–}^2P)$ line at 209 nm (+), the $B(^2S\text{–}^2P)$ line at 250 nm (●), and the $BCl(A\text{–}X)$ band (○) vs the incident electron energy.

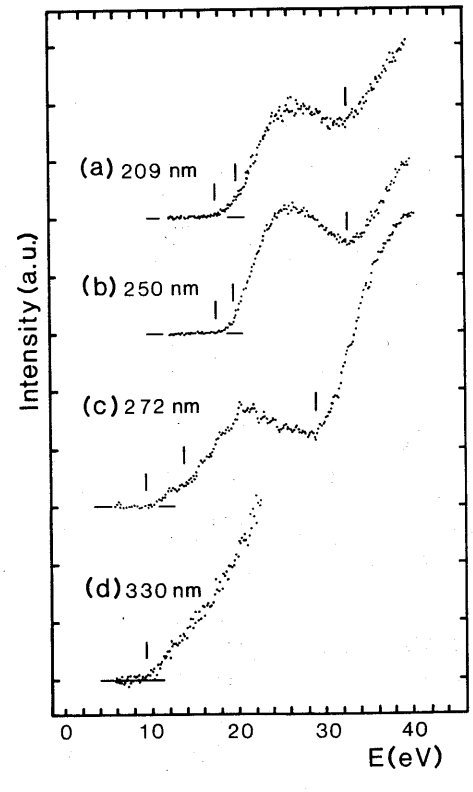

FIG. 5. The excitation functions of the fragments near their thresholds measured at (a) 209 nm, (b) 250 nm, (c) 272 nm, and (d) 330 nm. The vertical line indicates the observed onset.

TABLE II. Dissociation processes of BCl_3 and their thresholds.

Dissociation[a]	ΔH (eV) Calc.	Obs.[b]	Other data
(1) $BCl_3 \rightarrow B(3s\,^2S) + Cl_2 + Cl$	16.28		
(2) $BCl_3 \rightarrow B(3s\,^2S) + 3Cl$	18.70		
(3) $BCl_3 \rightarrow B(2s2p^2\,^2D) + Cl_2 + Cl$	17.25	17.7 ± 0.2	
(4) $BCl_3 \rightarrow B(2s2p^2\,^2D) + 3Cl$	19.67	20.0 ± 0.5	
(5) $BCl_3 \rightarrow B(2s2p^2\,^2D) + Cl_2 + Cl^+$	30.28		
		30–34	
(6) $BCl_3 \rightarrow B(2s2p^2\,^2D) + 2Cl + Cl^+$	32.70		
(7) $BCl_3 \rightarrow B(3p\,^2P^0) + Cl_2 + Cl$	17.34	17.7 ± 0.4	
(8) $BCl_3 \rightarrow B(3p\,^2P^0) + 3Cl$	19.76	19.7 ± 0.3	
(9) $BCl_3 \rightarrow B(3p\,^2P^0) + Cl_2 + Cl^+$	30.37		
		30–34	
(10) $BCl_3 \rightarrow B(3p\,^2P^0) + 2Cl + Cl^+$	32.79		
(11) $BCl_3 \rightarrow BCl(A\,^1\Pi) + Cl_2$	10.50		
(12) $BCl_3 \rightarrow BCl(A\,^1\Pi) + 2Cl$	12.92	13.9 ± 0.5	14.0 ± 1.5[c]
(13) $BCl_3 \rightarrow BCl(A\,^1\Pi) + Cl + Cl^+$	25.95	25–29	26 ± 2.5[c]
(14) $BCl_3 \rightarrow BCl_2^*(468\ nm) + Cl$	6.75[d]	7.0 ± 0.6	7.17[e]
(15) $BCl_3 \rightarrow BCl_2^*(330\ nm) + Cl$	8.90[d]	9.4 ± 0.4	9.80[e]

[a] Fragments without the electronic state represent their ground states.
[b] Uncertainties mean twice the standard deviation.
[c] Electron impact (Ref. 11).
[d] The lower limit based on the assumption that the lower state of the emission is the ground state.
[e] Photodissociation using synchrotron radiation (Ref. 9).

$BCl_3 \rightarrow B^* + Cl_2 + Cl^+$ and/or $BCl_3 \rightarrow B^* + 2Cl + Cl^+$ as shown in Table II.

The onsets at 271.5 nm are evaluated to be 9.4 ± 0.4 and 13.9 ± 0.5 eV. The 13.9 eV onset is ascribed to reaction (12) forming $BCl(A)$, whereas the onset at 9.4 eV is considerably lower than the calculated threshold for reaction (11). This onset, however, coincides with the value measured at 330 nm. Thus, we have concluded that the 9.4 eV onset is originated in the C band overlapped at 272 nm and that reaction (11) does not occur; in this connection, the ECSs in Table I and Fig. 4 are corrected for the overlapping C band. The second onset around 28 eV is mainly attributed to reaction (13), which has been mentioned by Jabbour, Martus, and Becker.[11] The $BCl(A)$ seems to be mainly produced via reactions (12) and (13). The ratio of reaction (12) to reaction (13) is estimated to be 1:3 at higher energies.

The onsets observed for the A and C bands are 7.0 ± 0.6 and 9.4 ± 0.4 eV, respectively, which agree well with each calculated threshold. This indicates that the upper state of the A band is lower than that of the C band and that the lower state for both bands is the ground state. The observed onsets agree well with the values obtained by photolysis of BCl_3 using synchrotron radiation.[9]

C. Radiative lifetimes of some fragments

Radiative lifetimes of several fragments have been measured at 209, 250, 272, and 300–342 nm. Almost all data are obtained at an impact energy of 100 eV because of the signal-to-noice ratio. Figure 6 shows typical time-dependent profiles of the delayed coincidence curve for boron atomic lines from BCl_3. These curves are analyzed as a superposition of three decaying components. Table III lists fluorescence lifetimes and magnitudes of three decaying components obtained for the same fragments; the magnitude means the relative photon count rate for each component. For BCl_2^*, the

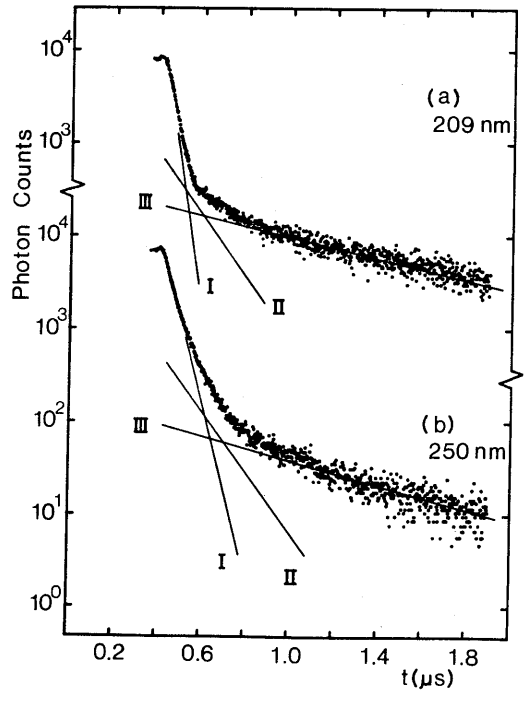

FIG. 6. Typical decay curves observed at 100 eV with the 3 nm FWHM resolution: (a) at 209 nm, (b) at 250 nm. Three lines represent the lifetime and amplitude of three decaying components.

TABLE III. Radiative lifetimes and their magnitudes for decay curves measured at 100 eV.

λ[a] (nm)	Transition	Component	Magnitude (%)	τ[b] (ns)	Assignment
209	$B(2s2p\ ^2D–^2P^0)$	I	49	27.5 ± 5	$B(2s2p^2\ ^2D)$
		II	23	130 ± 25	cascading
		III	27	760 ± 150	cascading
250	$B(3s\ ^2S–^2P^0)$	I	68	56 ± 4	$B(3p\ ^2P^0)$, cascading
		II	17	134 ± 30	
		III	16	640 ± 150	
272	$BCl(A\ ^1\Pi–X\ ^1\Sigma^+)$	I	55	22.4 ± 2	$BCl(A\ ^1\Pi)$
		II	20	100 ± 70	
		III	20	1200 ± 300	
300–342	BCl_2^*	I	6–11	23.7 ± 3	
		II	6–10	110 ± 70	
		III	83–86	1650 ± 200	BCl_2^*

[a] The band pass is 3 nm FWHM.
[b] The uncertainties mean twice the standard deviation.

presented values are an average of the lifetimes measured in the 300–342 nm region since the observed lifetimes did not apparently depend on the wavelength.

Three lifetimes obtained at 209 nm were 27.5 ± 5, 130 ± 25, and 760 ± 150 ns. The fastest value of 27.5 ± 5 ns is in reasonable agreement with the published lifetime of the $B(2s2p\ ^2D)$ state, 20 ns.[13] The slower components, which are considerably weaker than the fastest component, are attributable to cascading from upper states such as the $np\ ^2P^0$ and $nf\ ^2F^0$ states from the Grotrian diagram of boron.[13] We did not observe these cascadings since they seem to appear at the region longer than 600 nm.

The decay curve obtained at 250 nm was represented by superposition of three components with lifetimes of 56 ± 4, 134 ± 30, and 640 ± 150 ns. The lifetime of 56 ns, however, is remarkably longer than the lifetime of 3.6 ns for the $B(3s\ ^2S)$ state.[13] Component I is probably ascribed to cascading to the $B(3s\ ^2S)$ state from the $B(3p\ ^2P^0)$ state, of which lifetime is 50 ns.[13] Since no faster lifetime than 50 ns was observed at 250 nm, it is concluded that the $B(3s\ ^2S)$ state is not produced directly. This conclusion is consistent with the results of the excitation function as discussed in Sec. III B. Components I and II, which are considerably weaker than the fastest component, are attributable to either cascading from upper boron states or the tail of the *C* band overlapped.

The lifetime of component I, 22.4 ± 2 ns, obtained at 272 nm is in good agreement with the values 19.1 ± 2.0 ns obtained by the phase-shift method[10] and 18.8 ± 0.4 ns obtained by LIF of BCl produced by multiphoton dissociation of BCl_3.[5] Component III with the lifetime of 1200 ± 300 ns is probably attributed to the overlapping *C* band since the $BCl(A–X)$ emission produced by electron impact of 200 eV is cascade-free.[10]

The decay curves measured in the 300–342 nm region were analyzed as a superposition of three components with the lifetimes of 23.7 ± 3, 110 ± 70, and 1650 ± 200 ns. These values did not depend on the wavelength. Component III with the lifetime of 1.65 μs is the main component and is attributed to the *C* band. Components I and II, which are remarkably weaker than the main component, nearly disappear in the measurement at an incident electron energy of 30 eV. The lifetimes of components I and II are far shorter than the lifetime (2.6 μs)[13] of the $HCl^+(A\ ^2\Sigma^+–X\ ^2\Pi)$ band produced from impurity HCl. Thus, the faster components are probably affected by overlapping with Cl and Cl^+ atomic lines.

We did not measure the lifetime for the *A* band in the 400–580 nm region since stray photons from the tungsten filament become a serious problem. The reported lifetimes of the *A* band in the 440–660 nm region are 4.7–19.8 μs, which depend on the wavelength.[9] The lifetime obtained for the *C* band is considerably shorter than the value for the *A* band.

IV. SUMMARY

The light emissions from radiative fragments produced by low-energy electron impact on BCl_3 have been studied.

In the formation of the boron atom, the onset and lifetime measured at 209 nm agree well with the calculated threshold and the lifetime for the $B(2s2p^2\ ^2D)$ state, while the onset and lifetime measured at 250 nm are inconsistent with the calculated threshold and lifetime for the $B(3s\ ^2S)$ state. The values measured at 250 nm, however, agree well with the threshold and lifetime for the $B(3p\ ^2P^0)$ state. It is concluded that the $B(3s\ ^2S)$ state is produced by cascading via the $B(3p\ ^2P^0)$ state. Taking account of the magnitudes of component I in the corresponding decay curves, the formation cross sections for $B(2s2p^2\ ^2D)$ and $B(3p\ ^2P^0)$ are evaluated to be 2.4 ± 0.6 and $(3.0 \pm 0.5) \times 10^{-18}$ cm^2, respectively, at 100 eV. These boron states are produced by two reactions $BCl_3 \rightarrow B^* + Cl_2 + Cl$ and $BCl_3 \rightarrow B^* + 3Cl$ below 34 eV, while the reactions in which simultaneously a Cl^+ ion is produced become predominant above 40 eV.

From the observed onset forming $BCl(A\ ^1\Pi)$, the process $BCl_3 \rightarrow BCl(A) + 2Cl$ is main near its threshold, while the process $BCl_3 \rightarrow BCl(A) + Cl + Cl^+$ seems to be dominant above 28 eV.

For the BCl_2^* emission, it is concluded that the lower state for the *A* and *C* bands is the ground state. The lifetime

measured for the *C* band is remarkably shorter than the value for the *A* band observed by Suto *et al.*[9]

ACKNOWLEDGMENT

This study is partly supported by a Grant-in-Aid from the Ministry of Education, Science, and Culture.

[1] R. D. Verma, J. Mol. Spectrosc. **7**, 145 (1961).
[2] G. Pannetier, P. Goudmand, O. Dessaux, and I. Arditi, C. R. Acad. Sci. Paris **258**, 1201 (1964).
[3] H. Bredohl, I. Dubois, Y. Houbrechts, and P. Nzohabonayo, J. Phys. B **17**, 209 (1984).
[4] C. A. Moore, G. P. Davis, and R. A. Gottscho, Phys. Rev. Lett. **52**, 538 (1984).
[5] M. L. Mandich, C. E. Gaebe, and R. A. Gottscho, J. Chem. Phys. **83**, 3349 (1985).
[6] C. E. Gaebe, T. R. Hayes, and R. A. Gottscho, Phys. Rev. A **35**, 2993 (1987).
[7] R. A. Gottscho, Phys. Rev. A **36**, 2233 (1987).
[8] O. Dessaux, P. Goudmand, and G. Pannetier, C. R. Acad. Sci. Paris **265**, 480 (1967); Bull. Soc. Chim. France **1969**, 447.
[9] M. Suto, C. Ye, J. C. Han, and L. C. Lee, J. Chem. Phys. **89**, 6653 (1988).
[10] J. E. Hesser, J. Chem. Phys. **48**, 2518 (1968).
[11] Z. J. Jabbour, K. E. Martus, and K. Becker, Z. Phys. D **9**, 263 (1988).
[12] I. Tokue and Y. Ito, Chem. Phys. **125**, 347 (1988).
[13] A. A. Radzig and B. M. Smirnov, *Reference Data on Atoms, Molecules and Ions* (Springer, Berlin, 1985).
[14] T. Sato and T. Goto, Jpn. J. Appl. Phys. **25**, 937 (1986).
[15] B. Van Zyl, G. H. Dunn, G. Chamberlain, and D. W. O. Heddle, Phys. Rev. A **22**, 1916 (1980).
[16] W. L. Borst and E. C. Zipf, Phys. Rev. A **1**, 834 (1970).
[17] S. Trajmar and D. F. Register, in *Electron-Molecule Collisions*, edited by I. Shimamura and K. Takayanagi (Plenum, New York, 1984), p. 465.
[18] K. P. Huber and G. Herzberg, *Molecular Spectra and Molecular Structure IV. Constants of Diatomic Molecules* (Van Nostrand Reinhold, New York, 1979).
[19] A. N. Zaidel, V. K. Prokof'ev, and S. M. Raiskii, *Tables of Spectral Lines*, 3rd ed. (IFI/Plenum, New York, 1970).
[20] R. W. B. Pearse and A. G. Gaydon, *The Identification of Molecular Spectra*, 3rd ed. (Chapman and Hall, London, 1963).
[21] G. R. Möhlman and F. J. de Heer, Chem. Phys. **40**, 157 (1979).
[22] D. D. Wagman, W. H. Evans, V. B. Parker, R. H. Schumm, I. Halow, S. M. Bailey, K. L. Churney, and R. L. Nuttall, J. Phys. Chem. Ref. Data **11**, Suppl. 2 (1982).
[23] R. D. Srivastava and M. Farber, Trans. Faraday Soc. **67**, 2298 (1971).